

# Advanced Supersonic Parachute Inflation Research Experiment-2 (ASPIRE2) Parachute Modeling and Flight Mechanics Performance

Evan Roelke\*

*Analytical Mechanics Associates, Hampton, VA, 23681, USA*

Justin S. Green<sup>†</sup> and Soumyo Dutta<sup>‡</sup>

*NASA Langley Research Center, Hampton, VA, 23681, USA*

**The Advanced Supersonic Parachute Inflation Research Experiment-2 (ASPIRE2) program is designed to test and qualify the supersonic parachute for the Mars entry, descent, and landing stage of the Mars Sample Return campaign. The ASPIRE2 test was planned for early 2026 and would have involved testing the parachute at deployments of Mach 2.1 and higher load conditions than previous Mars missions. The ASPIRE2 simulation builds upon a previous test framework from the ASPIRE tests in 2017-2018 used to qualify the Mars 2020 parachute, but due to new requirements, the modeling and simulation for ASPIRE2 has needed development and characterization of different sensitivities. This paper looks at the mission design as of mid-2024 and presents the trade space for qualifying the parachute in a dynamic environment.**

## I. Introduction

THE qualification process for supersonic disk gap band (DGB) parachutes was recently refined to reduce risk as a result of canopy failures on two flight tests under the low density supersonic decelerator (LDS) campaign in 2015 and 2016 [1–3]. The advanced supersonic parachute inflation research experiment (ASPIRE) flight program was born out of this risk reduction activity, culminating in three sounding rocket flights in 2017 and 2018 to qualify the 21.5m DGB parachute deployed at Mach 1.85 and an opening load of around 35 kilo-pounds (kips) for the Mars 2020 flight [4, 5]. The successor to these flights is the Advanced Supersonic Parachute Inflation Research Experiment-2 (ASPIRE2) program, which builds off of the success of the ASPIRE program in an effort to qualify the 24m DGB parachute with a target deployment of Mach 2.1 or higher [6]. The Sample Retrieval Lander (SRL) segment of the Mars Sample Return (MSR) campaign is expected to be much heavier than the Mars 2020 entry capsule. As such, the SRL parachute will need to handle higher Mach and opening load conditions at deployment. ASPIRE2 is designed to produce these more extreme conditions. This paper provides an overview of the ASPIRE2 mission as of mid-2024 (prior to the NASA-led re-architecture studies of Fall 2024) and discusses the flight mechanics simulation development to support verification of mission requirements outlined at that time.

## II. Modeling and Simulation

This section will introduce the ASPIRE2 project in addition to discussing the development of the six-degree-of-freedom (6DOF) flight mechanics simulation, including atmospheric modeling, the guidance architecture, and parachute modeling. This simulation is developed using the Program to Optimize Simulated Trajectories II (POST2) for both the nominal trajectory and Monte Carlo simulations [7, 8]. POST2 is a generalized point-mass, rigid-body simulation that integrates translational and rotational equations of motion. The program offers multi-body support which is leveraged in this analysis to model the nosecone and parachute as separate entities. The simulation has a large heritage from Mars entry, descent, and landing missions, and has also been successfully applied to several Earth missions [9–12]. The POST2 simulation is used to predict the nominal and dispersed conditions at parachute deployment in addition to the vehicle’s trajectory through splashdown. The former is to ensure satisfactory test conditions and to tune onboard avionics, while the latter is used to station recovery assets and ensure range safety. Both of these predictions are used

---

\*Aerospace Engineer, Atmospheric Flight and Entry Systems Branch, MS 489, AIAA Member.

<sup>†</sup>Aerospace Engineer, Atmospheric Flight and Entry Systems Branch, MS 489, AIAA Member.

<sup>‡</sup>Aerospace Engineer, Atmospheric Flight and Entry Systems Branch, MS 489, AIAA Associate Fellow.

to support launch decisions. For configuration management between the systems engineering team and the modeling and simulation group, the simulation parameters are all tracked in a master parameter spreadsheet that contains all subsystem parameters, including mass properties, coordinate system definitions, hardware details, simulation constants, and more. This spreadsheet is parsed directly in the POST2 simulation to diminish risks of human error when defining input parameters.

### A. ASPIRE2 Concept of Operations

The concept of operations (CONOPS) of the ASPIRE2 mission are displayed in Figure 1, using blue text for ASPIRE2 metrics. For comparison purposes, data for the final ASPIRE mission, SR03, is displayed in red text. A schematic of the nosecone is displayed in Figure 2 [6]. Both missions were designed to launch from Wallops Flight Facility (WFF) using a two-stage sounding rocket, with Terrier serving as the first stage rocket. The second stage for ASPIRE2 (an Oriole rocket compared to the Black Brant vehicle used for SR03) ignites after achieving an altitude of roughly 4 km, burning out around 20.4 km. The payload separation event for ASPIRE2 occurs between 50-62 km (compared to 48.1 km on SR03). ASPIRE2 requires a higher apogee altitude to target the higher Mach and dynamic pressure requirements for this mission as compared to ASPIRE. The sounding rocket trajectory leading up to payload separation is modeled by WFF, who deliver the dispersed vehicle states at the payload separation point for further modeling and analysis in POST2 and the Dynamics Simulator for Entry, Descent, and Surface Landing (DSENDS), which serves as the independent verification and validation simulation for POST2. This paper will focus on the POST2 modeling, simulation development, and analysis.

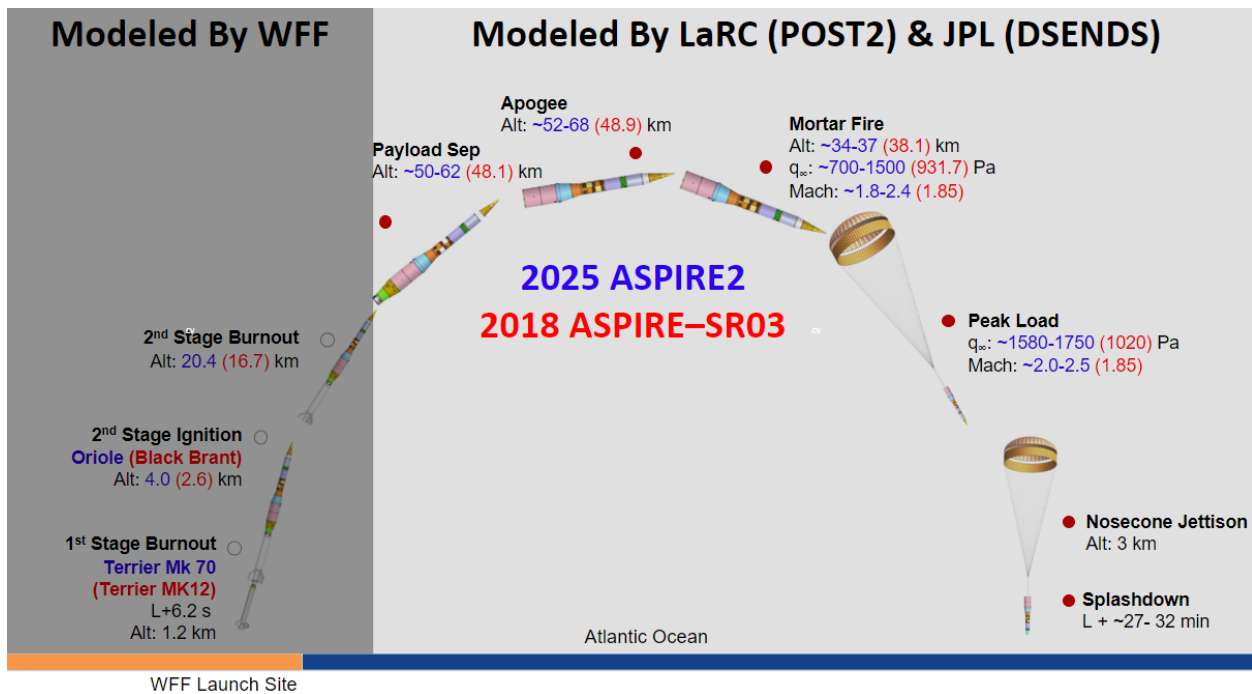


Fig. 1 ASPIRE2 concept of operations [13]

After the vehicle reaches its apogee between 52 and 66 km, the parachute mortar fire (MF) event is triggered between 34-37 km with the intent of targeting a dynamic pressure range of 700-1500 Pa and a Mach range of 1.8-2.4. This range is visualized in Figure 3, which depicts the Mach and dynamic pressure ranges of ASPIRE2 in blue as well as ASPIRE SR03 in red. These ranges are denoted as *Mach-Q* boxes. While there is overlap in the target requirements between ASPIRE and ASPIRE2, stars indicate the nominal targets to showcase the increased Mach and dynamic pressure values needed to qualify the parachute for the SRL mission.

One note about ASPIRE2 is that the program is targeting the highest performance area of the requirement Mach-Q box for the flight test, and thus the star for ASPIRE2 is not centered on the square [6]. The vehicle's guidance, the NASA Sounding Rocket Operations Contract (NSROC) Inertial Attitude Control System (NIACS) flight software (FSW),

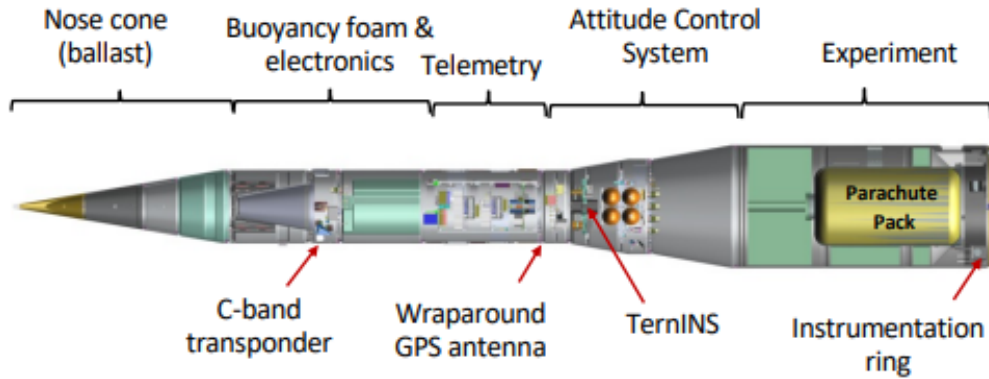


Fig. 2 ASPIRE2 vehicle configuration [6]

currently operates solely on a dynamic pressure target. This guidance capability is discussed further in Section II.C. As such, the nominal ASPIRE2 target dynamic pressure is currently set to 1400 Pa. The ascent trajectory is accordingly tuned by WFF to deliver separation states to nominally target a Mach number within the Mach-Q box. As shown in Figure 3, the current trajectory is targeting a Mach number at mortar fire of roughly 2.3.

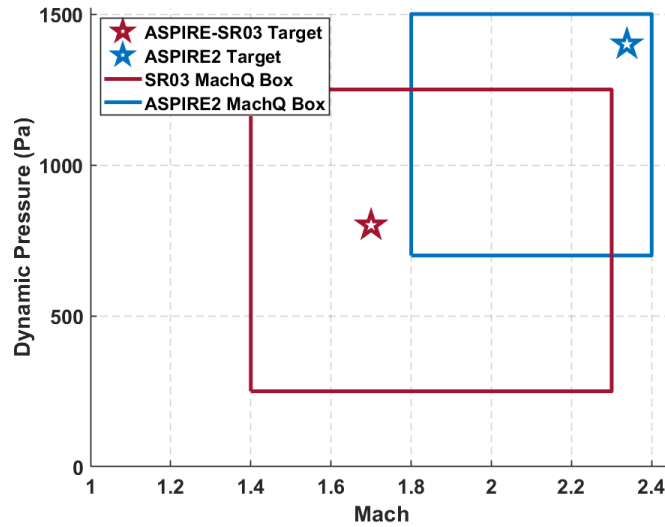


Fig. 3 Target Mach and dynamic pressure ASPIRE2 concept of operations

The NIACS flight software triggers the mortar fire after at least 4 consecutive dynamic pressure estimates at or above the target conditions. This trigger condition is denoted as a "software mortar fire" event, which is followed by a modeled delay of roughly 10 milliseconds before the "hardware mortar fire" event when the parachute bag physically begins to extract from the test article. The vehicle is required to attain a total angle of attack less than 5 degrees and attitude rates in all axes of less than 5 deg/s per axis at the time of the software mortar fire event.

The parachute inflation is modeled using an updated version of the model used for the Mars Science Laboratory (MSL) and Mars 2020 flights [14]. This model is discussed in more detail in Section II.D. There is a requirement on the vehicle to be able to test parachute performance up to 1.4 times the load required for the SRL mission (currently 70-140 kips) [15, 16]. In addition, outcomes of the Low Density Supersonic Decelerator (LSD) campaign have prompted a requirement that the parachute canopy must be fully visible in the camera fields of view throughout the inflation event. This paper does not cover the parachute visibility details, deferring to Ref. [17] for more in-depth analysis of this requirement.

Following parachute inflation, the test article descends on the parachute until it reaches an altitude of 3 km, at which point the nosecone is jettisoned, with splashdown finally occurring after a mission elapsed time of roughly 27-32 minutes.

## B. Atmospheric Profile

The atmospheric profile and associated uncertainties are large drivers in flight software performance and splashdown location prediction accuracy. The NIACS flight software also relies on accurate atmospheric estimates of density and wind speeds for control capability, with further discussion being found in Section II.C. Consequently, the POST2 simulation incorporates forecast data from NASA’s Goddard Earth Observation System Version 5 (GEOS-5) which is operated by NASA Goddard Space Flight Center’s (GSFC) Global Modeling and Assimilation Office (GMAO) [18, 19]. The GEOS-5 forecast data is used to obtain atmospheric parameters for the range near Wallops Flight Facility and used to tune parameters for the flight software. However, it is infeasible to estimate the atmospheric conditions on the exact day of launch while doing this analysis years before the launch. Instead, the current year’s forecast within the same month as the expected launch date is used to try and capture monthly mean deviations in atmospheric data but also prepare the simulation framework to easily ingest forecast data leading up to the actual launch. This enables the simulation team to not only get more accurate trajectory expectations for the day of launch, but also to get an increasingly-accurate estimate of the various component splashdown ellipses for the recovery teams.

Previous projects, including ASPIRE, used climatological predictions, such as those by EarthGRAM 2010 [20], to design preliminary trajectories and then switched to GEOS-5 closer to operations. Ref. [21] contains examples of this workflow for ASPIRE and other recent Earth EDL missions. However, the climatological models have large dispersions for their atmospheric properties, leading to large uncertainties for key metrics like parachute deployment, dynamic pressure, and structural loads. Since the ASPIRE experience showed that forecast atmospheric models, like GEOS-5, would eventually decrease the dispersion for operations, ASPIRE2 has adopted similar atmospheric model integration processes.

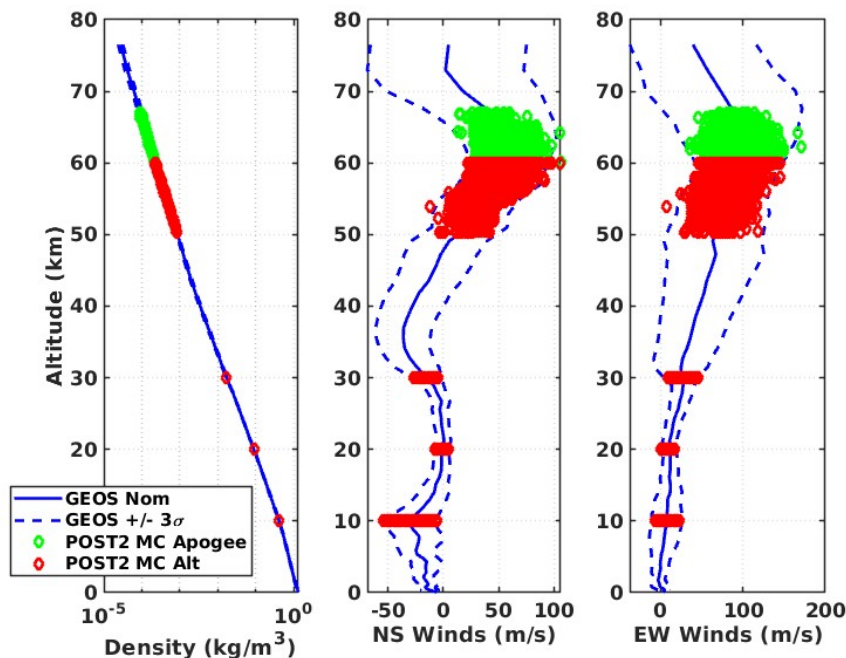


Fig. 4 POST2 atmospheric data within GEOS-5 data

The GEOS-5 predictions are parsed at a set of given pressure levels to generate nominal and dispersed atmospheric parameter tables to be fed into the simulation as the truth model. Figure 4 showcases an example GEOS-5 forecast nominal and  $\pm 3\sigma$  (Gaussian distribution) bounds for density and winds in blue. The POST2 atmospheric parameters parsed throughout a candidate set of monte carlo trajectories are shown in green and red, with the former representing

data points captured up to apogee and the latter representing data points post-apogee. This shows good agreement between the GEOS forecast and the POST2 output, which is useful for validating the POST2 implementation. This example forecast also shows high wind speeds at upper altitudes, which can cause significant drift as the vehicle descends on the parachute. This reinforces the desire to have precise simulation atmospheric estimates; while conservative estimates are useful for bounding trajectory performance, accurate trajectory profile estimates are necessary for range safety considerations.

### C. Guidance, Navigation, and Control

The vehicle is equipped with the NSROC Inertial Attitude Control System (NIACS) flight software. The flight software was provided by WFF and integrated into the POST2 simulation. The flight software is responsible for signalling the parachute mortar fire event in addition to attitude control system (ACS) leading up to mortar fire. The attitude control employs cold-gas thrusters that receive commands from the NIACS software in an effort to limit vehicle attitude rates and angle of attack in the face of atmospheric and navigation uncertainties. Mission requirements specify the vehicle’s total angle of attack must be less than  $5^\circ$  and each axis’ angular rate must be within  $\pm 5^\circ$ . The vehicle is equipped with 8 yaw/pitch control thrusters in addition to 4 roll control thrusters. Four of the yaw/pitch actuators are reserved for high level (or super) control [22].

The NIACS flight software’s attitude control performance relies on accurate estimates of the ambient environment to ensure proper control outputs. Otherwise, the vehicle’s attitude at mortar fire may be outside the requirement bounds, or in the extreme case the vehicle may run out of ACS fuel. These estimates of the atmospheric density and winds are in the form of 6th order polynomial approximations. Previous work on the ASPIRE campaign led to the selection of 6th order as a sufficient choice that also met the mathematical library and coding requirements for the flight software. The use of curve fits within the flight software as opposed to a table look-up is needed for computational efficiency. Figure 5 shows the percent difference between the true GEOS-5 nominal atmospheric density and the polynomial fit in the area of interest for the ASPIRE2 flights. In general there is good agreement between the two profiles, with differences being less than 2% at all altitudes and the difference reducing as the altitude approaches that of the mortar fire event at approximately 40 km. Testing the flight software within a Monte Carlo simulation in POST2 allows one to compare the flight performance when simulating off-nominal conditions, such as higher-than-expected density or off-nominal aerodynamics. Robust performance margins in the simulation improve confidence in the flight software’s ability to control the vehicle leading up to the mortar fire event.

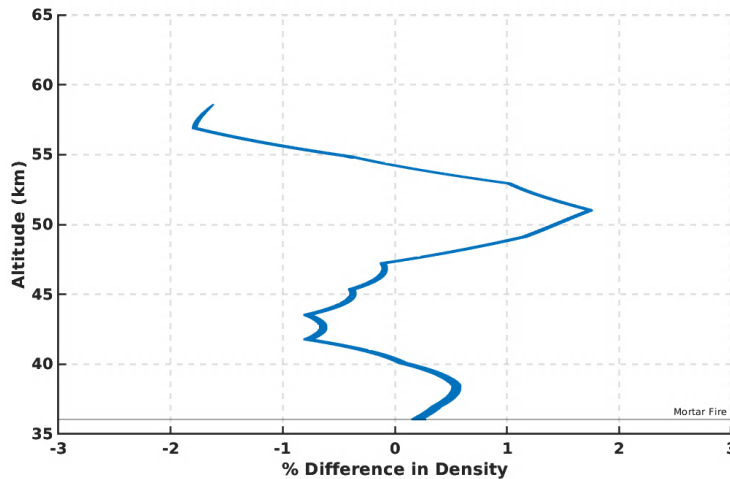


**Fig. 5 Percent difference between truth GEOS data and NIACS polynomial fit**

Using these polynomial curve fits and the vehicle navigated state, the NIACS flight software also estimates dynamic pressure to support the mortar fire trigger event. At least 4 consecutive dynamic pressure estimates at or above the targeted value are required in order to trigger the software mortar fire.

#### D. Parachute Modeling

This section discusses the parachute model updates that ASPIRE2 has incorporated as compared to the ASPIRE campaign. This updated parachute model, denoted as the Mars 2020 parachute model, was born out of lessons learned during the LDSO campaign [1, 14]. This program uncovered gaps in parachute testing methodology, leading to increased perception of risk for Mars 2020 parachute design. Coupled with the fact that the Mars Science Laboratory mission flew at what was believed to be very low margins after the fact, a new parachute model was needed. Specifically, LDSO testing implied that the peak canopy stress did not necessarily correlate with peak parachute load, suggesting that the drag force generated by the canopy was not well correlated with canopy stress. In addition, LDSO indicated that higher canopy stresses could be generated than those predicted with previous models even when additional factors of safety were applied in an attempt to account for additional dynamics that could be encountered during supersonic inflation. Finally, subsonic testing of the fully-open canopy at an enhanced load does not yield enough evidence that the canopy could survive a supersonic inflation event at, or even below, the flight limit load [1].

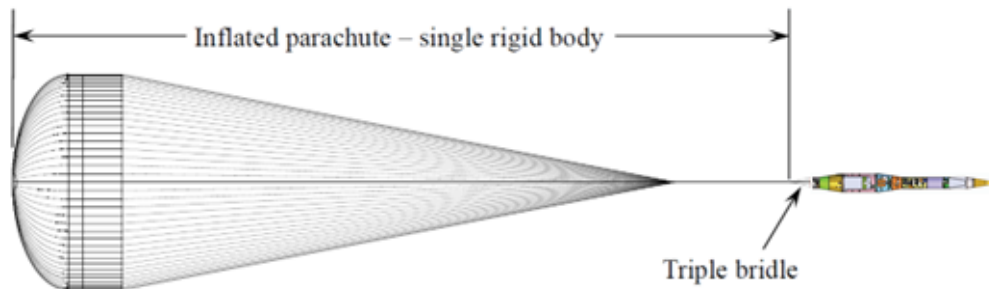


**Fig. 6 Schematic of the fully inflated parachute relative to the ASPIRE2 vehicle**

These discoveries led to the inception of the Mars 2020 parachute model, which has been integrated into the ASPIRE2 simulation for this analysis\*. A key difference in this model is that the parachute bag dynamics being ejected out of the canister is not simulated. Even though the ASPIRE model of simulating the constraint forces on the parachute in a can is derived in physics, parachute ejection and spawning is empirically tuned to flight observations in the Mars 2020 model.

In ASPIRE2, the timing between mortar fire and line stretch is computed directly based on the fully stretched-out parachute length and the average deployment bag speed, which depends on the mortar muzzle velocity based on work from Ref. [23]. This parachute opening distance is parameterized to match observations of parachute opening from previous DGB flights. At line stretch, the parachute vehicle is spawned into existence (colloquially referred to as "apparation") in the simulation with an initial dispersed velocity as well as total angle of attack cone and clock angles relative to the nosecone's body coordinate system [24].

Another difference between the ASPIRE and the Mars 2020 parachute model is the computation of peak parachute opening load, which is computed according to:

$$F_{peak} = 2k_P q_\infty S_P \quad (1)$$

where  $k_P$  is the momentum peak opening load factor,  $q_\infty$  is the dynamic pressure at the parachute's center of mass, and  $S_P$  is the projected area of the parachute. The derivation of this method is discussed in Ref. [25]. The variation of parachute forces and moments uses a legacy area oscillation model developed using flight data from Viking BLDT AV-4 and Mars Phoenix flights. More information on the legacy parachute models can be found in Ref [24].

The Mars 2020 parachute model is a behavior-based model that attempts to capture expected behavior rather than being tied to a specific physics model. This allows several parameters to be tuned to match behavioral expectations; one example is the parachute's initial area ratio. This parameter is tuned with the intent that the initial force on the parachute canopy is large enough to prevent the relative distance between the primary vehicle and parachute from decreasing prior to full inflation. In other words, the expectation throughout inflation is that there should be tension in at least one of the three elastic bridle line connections between the parachute and test article. The parachute area ratio,  $k_1$ , is computed as follows:

\*The parachute model is outlined in the memo entitled "Description of the Parachute Models Used in the POST2 and DSENDS End-to-End Simulations v10" by Juan R. Cruz, David W. Way, and Carlie H Zumwalt of NASA Langley Research Center and Clara O'Farrell, Christopher L. Tanner, and Ian G. Clark of the Jet Propulsion Laboratory, September 15, 2021"

$$k_1 = \max \left[ k_1^0, \left( \frac{t - t_{LS}}{t_{FI} - t_{LS}} \right)^n \right] \quad (2)$$

where  $k_1^0$  is the initial area ratio,  $t$  is time,  $t_{LS}$  and  $t_{FI}$  are the times of line stretch and full inflation, respectively, and  $n$  is a chosen power law exponent which determines the speed of inflation and typically chosen to be 4. Equation 2 varies between  $k_1^0$  and 1.0 and is used to scale the parachute force when computing parachute static aerodynamic force and moment coefficients. Figure 7 shows the evolution of the parachute area ratio and the parachute drag force plotted against time. Note that until the power law component of Equation 2 exceeds the initial area ratio,  $k_1$  is assumed to be constant. This is suitable for the behavior-based approach of the Mars 2020 parachute model because the goal is to ensure there is tension in the bridle lines as opposed to attempting to match an expected parachute force at the beginning of inflation. Section III.A will go into more detail about how the initial area ratio was selected for the ASPIRE2 flight.

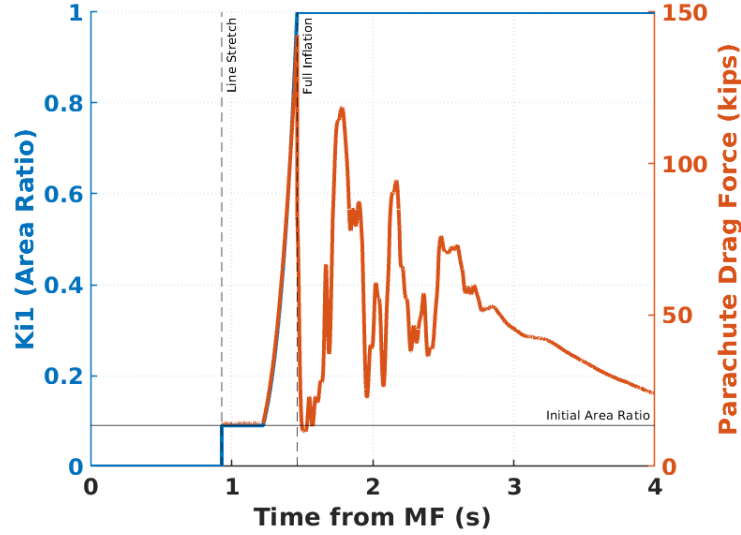


**Fig. 7 Initial area ratio vs. parachute drag force**

As previously mentioned, during the inflation event, the parachute static aerodynamic force and moment coefficients are computed in part from the initial area ratio during the inflation event. Both during inflation and post-inflation, the static force and moment coefficients are scaled by a Mach efficiency factor (MEF) that relates the static coefficients usually computed for a low Mach number to its equivalent higher Mach number value. The MEF derivation is described in detail in Ref. [24]. The MEF is interpolated in the POST2 simulation from a set of tables as a function of Mach number. Figure 8 shows the Mach efficiency factor values output from the POST2 simulation plotted against the expected bounds of the MEF tables (shown in black) for a nominal trajectory and dispersed case. The POST2 data is colored by relevant parachute event, with red data points corresponding to during inflation, blue as between full inflation to Mach 1.4, and magenta below Mach 1.4 (where the area oscillation model is disabled in the simulation).

The parachute aerodynamic coefficients are also provided as tables indexed on total angle of attack, being interpolated in the model and scaled by MEF. During inflation, these coefficients are scaled by:

$$k_2 = \frac{F_{peak} k_1}{q_\infty S_0 \sqrt{C_T^2 + C_N^2 + C_Y^2}} \quad (3)$$

where  $S_0$  is the nominal parachute area ratio,  $C_T$  is the tangential force coefficient,  $C_N$  is the normal force coefficient, and  $C_Y$  is the side force coefficient. Once the parachute reaches full inflation, the coefficients are instead scaled by  $\frac{C_D}{C_D^0}$ , where  $C_D$  is the drag coefficient and  $C_D^0$  is the nominal drag coefficient. Previous work modeled the static aerodynamic coefficients for ASPIRE using wind tunnel tests to characterize wake effects behind slender bodies and reduce aerodynamic uncertainty at subsonic speeds [5]. Figure 9 shows nominal aerodynamic coefficients relative to total angle of attack for the tangential ( $C_T$ ), normal ( $C_N$ ), and pitching moment about the suspension line confluence

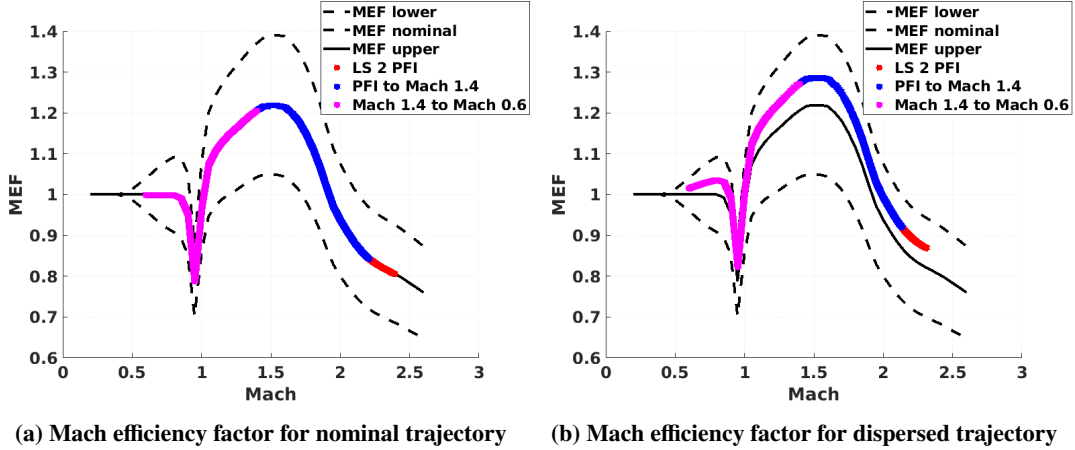


Fig. 8 Mars 2020 mach efficiency factor

point ( $C_{M,0}$ ) relative to the model bounds. For each dispersed Monte Carlo case the curve is shifted above or below the nominal bound. More information on the static aerodynamic coefficient calculations can be found in Ref. [24]. This figure shows that the POST2 output is meeting the expectations of the model, giving confidence in the results presented in Section III.

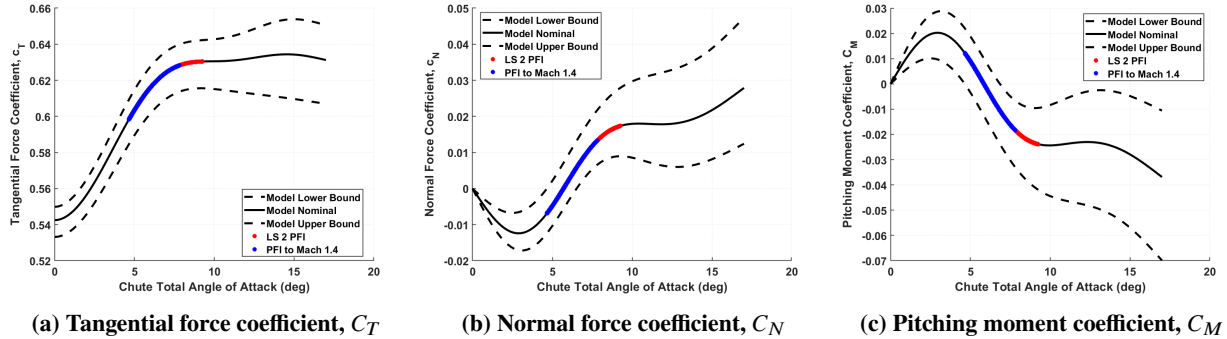


Fig. 9 Parachute static aerodynamic coefficients

This section briefly covered the basics of the Mars 2020 parachute model and discussed the key differences in this model as compared to previous parachute models. The POST2 model outputs for a few key variables were plotted against expected model boundaries to demonstrate proper integration and give confidence in the results presented in this paper. Section III will cover the parachute tuning parameter selection in addition to flight mechanics and parachute Monte Carlo performance.

### III. Results

This section covers the parachute and flight mechanics performance of the ASPIRE2 vehicle as of mid-2024. Monte Carlo methods are used within POST2 to simulate 8000 dispersed trajectories. Section III.A will present parachute performance, Section III.B details flight mechanics performance and mission requirement assessment, and Section III.C shows some preliminary range safety analysis.

#### A. Parachute Performance

This section covers the performance of the ASPIRE2 parachute with respect to the mission requirements. It also covers sensitivity studies related to the initial area ratio,  $k_1^0$ , selection. Recall from Section II.D that the  $k_1^0$  is a tuning parameter intended to maintain tension in at least one elastic bridle line during inflation. A major consideration during

the implementation of the Mars2020 parachute model was how to select an appropriate  $k_1^0$  value.

Figure 10 outlines the trade study involved to arrive at a reasonable answer to this problem. More specifically, Figure 10b shows the atmospheric-relative velocity vs. time since mortar fire for various initial area ratios plotted against the SRL simulation (black), which at the time employed a 3% initial area ratio. However, if the same value is applied to ASPIRE2, the nominal trajectory contains periods of time during inflation where each elastic bridle line is tension-less. This is depicted in Figure 10a, which shows the line deflection of each bridle line as a function of time since mortar fire (blue), overlaid with a boolean indicator (orange) that is false if at least one elastic line is in tension and true otherwise.

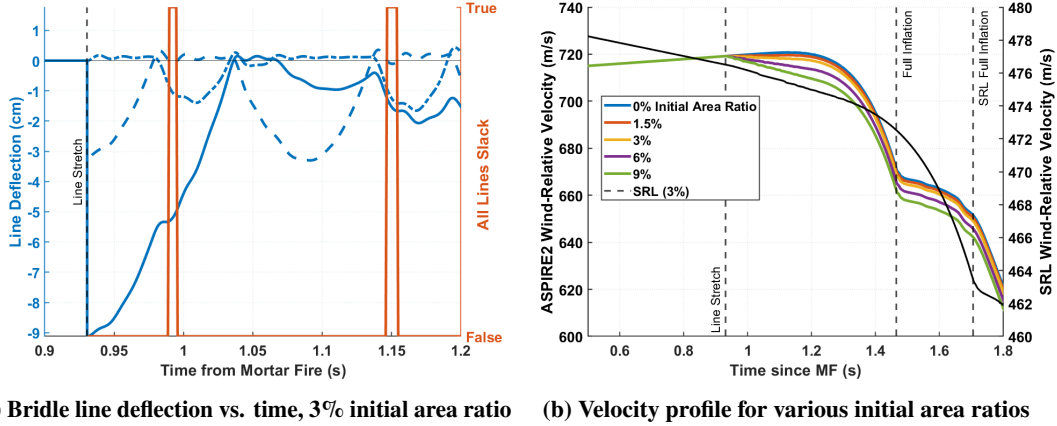


**Fig. 10 ASPIRE2 initial area ratio considerations**

It is apparent that a 3%  $k_1^0$  is an insufficient value for the ASPIRE2 vehicle; However, Figure 10b holds an explanation for this behavior. The plot shows atmospheric-relative velocity as a function of time since mortar fire for various  $k_1^0$  values compared to the SRL simulation (black). While the SRL vehicle is decelerating through line stretch, the ASPIRE2 vehicle is shown to be accelerating through the same event at low initial area ratio values. This is due to the fact that the SRL vehicle is blunt-bodied and therefore has a lower ballistic coefficient, experiencing drag more so than the slender-bodied ASPIRE2 test article. It is only when  $k_1^0$  reaches roughly 6% that the vehicle is slowed down at line stretch due to the immediate drag force from the parachute. Furthermore, it is noted that the slope of the velocity curve matches that of the SRL simulation for a  $k_1^0$  value of 9%.

This observation is investigated further in Figure 11a, which shows trade study Monte Carlo results of the percent of time all bridle lines were slack (tension-less) during inflation for a set of initial area ratios. The overall distributions are depicted using Gaussian quantiles to better highlight outliers and the distribution growth as a function of case number. As the initial area ratio increases, the percent slack time reduces overall. The 99%-tile value is shown to drop below 1% for a  $k_1^0$  value of 9%.

Combining this aspect with the match in SRL vehicle slope in Figure 10b, the initial area ratio for ASPIRE2 was chosen to be 9%. Figure 11b shows the same parameters as Figure 10a but for a nominal trajectory with  $k_1^0$  set to 9%. This shows that the nominal ASPIRE2 trajectory with the selected  $k_1^0$  value maintains tension in at least one elastic bridle line during inflation; however, further analysis is needed to verify the selected  $k_1^0$  would produce the expected outcome in flight.

The Monte Carlo statistics for parachute peak opening load are shown in Figure 12. Note that the initial mission maximum load limit required was 140 kips [6]. This is marked by a magenta line in Figure 12, and it is apparent that a non-negligible number of cases exceed that maximum load limit; however, this requirement value is subject to change: for instance, targeting a lower dynamic pressure and/or Mach number target would reduce the peak parachute opening load, or perhaps the max test load limit would increase. Regardless, these results indicate that the vehicle is capable of targeting up to and above the maximum test load limit.

## B. Flight Mechanics Monte Carlo Performance

This section presents the ASPIRE2 flight mechanics performance Monte Carlo results. Figure 13 presents the results for two primary mission requirements: the total angle of attack and vehicle attitude rates at mortar fire. Figure 13a shows the Gaussian quantiles of the total angle of attack for each Monte Carlo case, while Figure 13b shows the vehicle

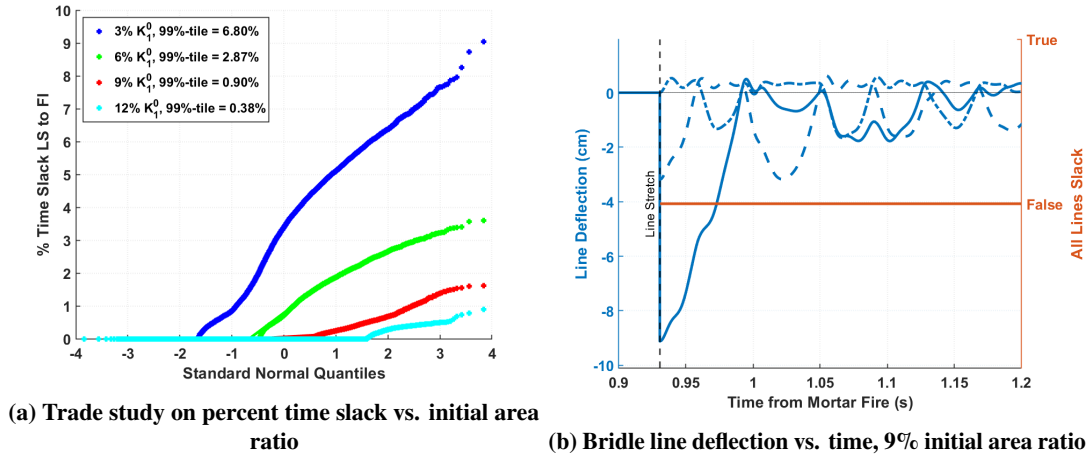


Fig. 11 ASPIRE2 parachute vent trace inside effective fields of view

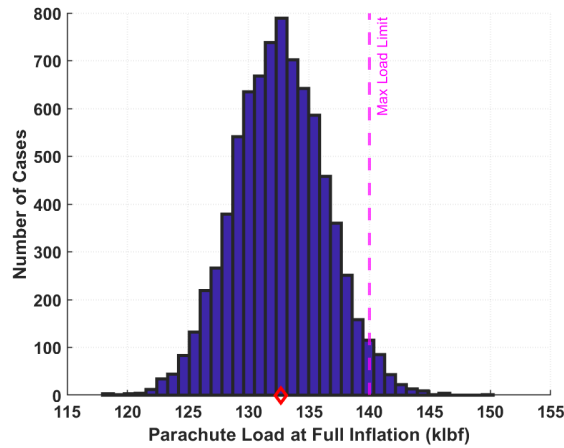


Fig. 12 Peak parachute opening load statistical results

roll rate, pitch rate, and yaw rate at mortar fire. The mission requirements state that the 99th %-tile of total angle of attack must be less than 5 degrees while the attitude rates must be within  $\pm 5 \text{ deg/s}$ , which are marked by magenta lines in the plots.

Figure 13 shows that the ASPIRE2 vehicle is meeting all flight mechanics mortar fire stability requirements, with 100% of cases lying within the specified bounds. Note that the pitch and yaw rates are overlaying one another in Figure 13b. These results suggest that the NIACS flight software has good knowledge of the atmosphere and vehicle state to provide sufficient attitude control. In addition, there is apparent margin in terms of vehicle stability that would potentially alleviate some constraints on vehicle mass properties of allocated ACS fuel requirements, if required in future design iterations.

Meanwhile, Figure 14 plots Monte Carlo data of dynamic pressure and Mach number at mortar fire relative to the Mach-Q box defined introduced in Figure 3. The nominal and target Mach-Q values are plotted as a yellow square and red diamond, respectively. The slight offset from the target condition is a result of the simulated delay between "software" and "hardware mortar fire" as well as the "software" mortar fire being triggered by 4 consecutive estimates at or above the target value.

While Figure 14 shows a non-negligible number of Monte Carlo cases lying outside the Mach-Q box, the only mission requirement related to Mach-Q box targeting concerns nominal trajectory capability, although this too is subject to change. In addition, the current trajectory is targeting the upper corner of the Mach-Q box, which offers significant design margin should the ascent trajectory need to be refined to target a lower dynamic pressure and/or Mach number at

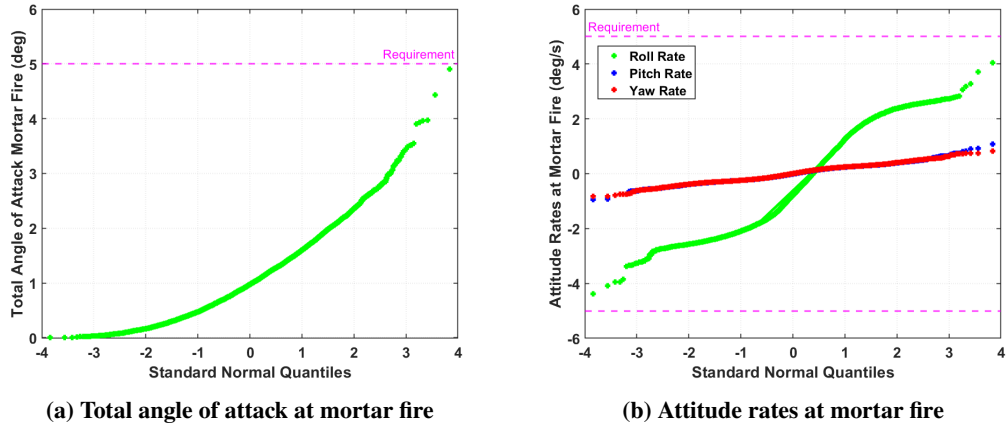


Fig. 13 ASPIRE2 mortar fire performance

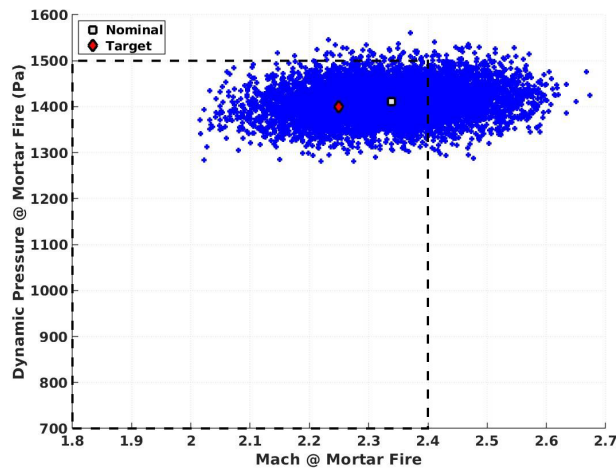
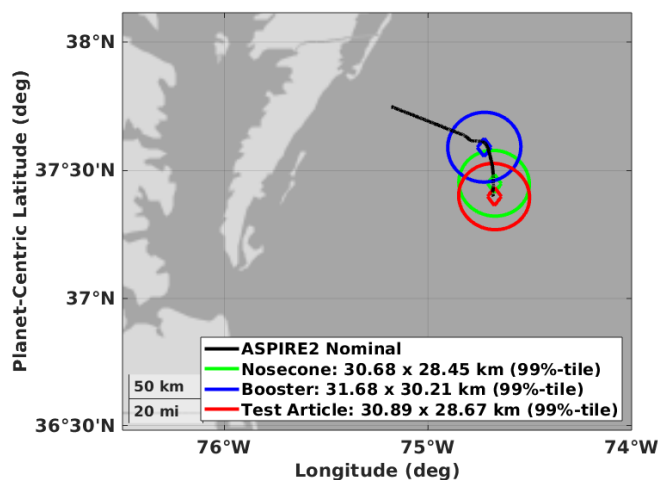


Fig. 14 Dynamic Pressure vs. Mach number Monte Carlo results

mortar fire.

### C. Range Safety and Splashdown Predictions

This section presents range safety results for the ASPIRE2 mission. Figure 15 plots the nominal vehicle groundtrack between separation and splashdown, overlaid on Monte Carlo ellipses of the booster (blue), nosecone (green) that is jettisoned 3km above the surface, and the test article (red). Figures such as this are useful for planning test article recovery as well as understanding probably debris locations during the flight to ensure there is no risk to the public.



**Fig. 15 Vehicle nominal trajectory and Monte Carlo splashdown footprint**

#### IV. Conclusion

This paper discusses the ASPIRE2 six degree-of-freedom flight mechanics simulation modeling and development as of mid-2024 prior to the NASA-led Mars Sample Return campaign re-architecture studies. Sub-systems including the atmospheric model, parachute model, and guidance, navigation, and control were discussed in the context of their implementation within the flight mechanics simulation. Initial parachute system results are presented and the selection of various tuning parameters is discussed. This work also shared initial flight mechanics performance results, providing assessments relative to mission requirements. Initial results showed that the ASPIRE2 vehicle meets all angle of attack and attitude rate requirements at the mortar fire event, in addition to being capable of enveloping the qualification target.

#### Acknowledgments

The authors would thank the flight mechanics and aerosciences teams for the ASPIRE2 project and Larry Coy and Robert Luchessi of NASA Goddard Flight Center for help with usage of forecast models, such as GEOS-5.

#### References

- [1] Tanner, C. L., Clark, I. G., and Chen, A., "Overview of the Mars 2020 parachute risk reduction activity," *2018 IEEE Aerospace Conference*, 2018, pp. 1–11. <https://doi.org/10.1109/AERO.2018.8396717>.
- [2] Clark, I. G., Gallon, J. C., and Witkowski, A., "Parachute decelerator system performance during the low density supersonic decelerator program's first supersonic flight dynamics test," *23rd AIAA Aerodynamic Decelerator Systems Technology Conference*, 2015, p. 2130.
- [3] O'Farrell, C., Brandeau, E. J., Tanner, C., Gallon, J. C., Muppidi, S., and Clark, I. G., "Reconstructed parachute system performance during the second LDSD supersonic flight dynamics test," *AIAA Atmospheric Flight Mechanics Conference*, 2016, p. 3242.
- [4] Dutta, S., Karlgaard, C. D., Tynis, J. A., O'Farrell, C., Sonneveldt, B. S., Queen, E. M., Bowes, A. L., Leylek, E. A., and Ivanov, M. C., "Advanced supersonic parachute inflation research experiment preflight trajectory modeling and postflight reconstruction," *Journal of Spacecraft and Rockets*, Vol. 57, No. 6, 2020, pp. 1387–1407.
- [5] Dutta, S., "ASPIRE Parachute Modeling and Comparison to Post-Flight Reconstruction," *AIAA Scitech 2020 Forum*, 2020. <https://doi.org/10.2514/6.2020-0756>.
- [6] O'Farrell, C., Leylek, E. A., Lobbia, M. A., and Siegel, K. J., "ASPIRE2: The Mars Sample Retrieval Lander's Supersonic Parachute Test Program," *2023 IEEE Aerospace Conference*, 2023, pp. 1–9. <https://doi.org/10.1109/AERO55745.2023.10115818>.

- [7] Striepe, S., Powell, R., Desai, P., Queen, E., Way, D., Prince, J., Cianciolo, A., Davis, J., Litton, D., Maddock, R., Shidner, J., Winski, R., O'Keefe, S., Bowes, A., Aguirre, J., Garrison, C., Hoffman, J., Olds, A., Dutta, S., Zumwalt, C., White, J., Brauer, G., Marsh, S., and Engel, M., *Program To Optimize Simulated Trajectories II (POST2), Vol. II: Utilization Manual*, Version 3.0.NESC, 2015.
- [8] Williams, R. A., Lugo, R. A., and Hoffman, J. A., "Design of an Application Programming Interface for the Program to Optimize Simulated Trajectories II," AIAA 2024-0161, *AIAA SciTech Forum*, Orlando, FL, 2024. <https://doi.org/10.2514/6.2024-0161>.
- [9] Maddock, R. W., Cianciolo, A. M. D., Litton, D. K., and Zumwalt, C. H., "InSight Entry, Descent, and Landing Preflight Performance Predictions," *Journal of Spacecraft and Rockets*, Vol. 58, No. 6, 2021, pp. 1590–1600.
- [10] Dutta, S., Way, D. W., Zumwalt, C. H., and Blette, D. J., "Postflight Assessment of Mars 2020 Entry, Descent, and Landing Simulation," *Journal of Spacecraft and Rockets*, Vol. 61, No. 3, 2024, pp. 847–857.
- [11] Deshmukh, R., Dutta, S., Bowes, A., and DiNonno, J., "Flight Mechanics Analysis of Low-Earth Orbit Flight Test of an Inflatable Decelerator," *AIAA SCITECH 2024 Forum*, 2024, p. 1501.
- [12] Francis, S. R., Johnson, M. A., Queen, E., and Williams, R. A., "Entry, Descent, and Landing Analysis for the OSIRIS-REx Sample Return Capsule," *46th Annual AAS Guidance, Navigation and Control (GN&C) Conference*, 2024.
- [13] Justin S. Green, E. A. L., Evan Roelke, and Kline, C., "Advanced Supersonic Parachute Inflation Research Experiment - 2 (ASPIRE2) Flight Mechanics Modeling and Simulation," *International Planetary Probe Workshop (IPPW)*, 2023.
- [14] Cruz, J. R., Way, D. W., Shidner, J. D., Davis, J. L., Adams, D. S., and Kipp, D. M., "Reconstruction of the Mars Science Laboratory Parachute Performance," *Journal of Spacecraft and Rockets*, Vol. 51, No. 4, 2014, pp. 1185–1196. <https://doi.org/10.2514/1.A32816>.
- [15] Siegel, K. J., O'Farrell, C., Rowan, J., Peterson, K., and Lowry, C., "Preliminary Design of the Supersonic Disk-Gap-Band Parachute for Sample Retrieval Lander," *AIAA AVIATION FORUM AND ASCEND 2024*, 2024, p. 4222.
- [16] Peterson, K., Siegel, K. J., Whalen-Muse, K., O'Farrell, C., Lowry, C., and Kester, M., "Sample Retrieval Lander Parachute System Deployment Test Campaigns: Modeling, Testbed Development, and Intermediate Results," *AIAA AVIATION FORUM AND ASCEND 2024*, 2024, p. 4327.
- [17] Evan Roelke, R. A. W. S. D., Justin S. Green, and Andreini, M., "Shape Approximation in Camera Fields of View for Parachute and Descent Imaging Visibility Applications," *Presented at the 2025 SciTech Conference*, 2025.
- [18] Molod, A., Takacs, L., Suarez, M., Bacmeister, J., Song, I., and Eichmann, A., "The GEOS-5 Atmospheric General Circulation Model: Mean Climate and Development from MERRA to Fortuna," Tech. Rep. NASA TM 2012-104606-VOL-28, NASA GFSC, 2012.
- [19] Rienecker, M. M., Suarez, M. J., Todling, R., Bacmeister, J., Takacs, L., Liu, H.-C., Gu, W., Sienkiewicz, M., Koster, R., Gelaro, R., Stajner, I., and Nielsen, J., "Guide to Meteorological Instruments and Methods of Observation," Tech. rep., The GEOS-5 Data Assimilation System - Documentation of Versions 5.0.1, 5.1.0, and 5.2.0, 2008.
- [20] White, P., and Hoffman, J., "Earth Global Reference Atmospheric Model (Earth-GRAM): User Guide," Tech. rep., TM 2021-0022157, 2021.
- [21] Dutta, S., "Use of Forecast Atmospheric Data for Earth Entry, Descent, and Landing Missions," *Journal of Spacecraft and Rockets*, 2024. <https://doi.org/10.2514/1.A36119>.
- [22] Dutta, S., Queen, E., Bowes, A., Leylek, E., and Ivanov, M., "ASPIRE Flight Mechanics Modeling and Post Flight Analysis," *2018 Atmospheric Flight Mechanics Conference*, June 2018. <https://doi.org/10.2514/6.2018-3625>, URL <https://arc.aiaa.org/doi/abs/10.2514/6.2018-3625>.
- [23] Greene, G., "Opening Distance of a Parachute," *Journal of Spacecraft*, Vol. 7, No. 1, 1970, pp. 98–100. <https://doi.org/10.2514/3.29878>.
- [24] Cruz, J. R., Way, D., Shidner, J., Davis, J. L., Powell, R. W., Kipp, D., Adams, D. S., Sengupta, A., Witkowski, A., and Kandis, M., "Parachute models used in the Mars Science Laboratory entry, descent, and landing simulation," *AIAA Aerodynamic Decelerator Systems (ADS) Conference*, 2013, p. 1276.
- [25] Way, D., "A Momentum-Based Indicator for Predicting the Peak Opening Load of Supersonic Parachutes," IEEE Paper No. *IEEE Aerospace Conference*, Big Sky, MT, 2018.